ACS OMEGA

http://pubs.acs.org/journal/acsodf

Article

Development of Low-Cost Porous Carbons through Alkali Activation of Crop Waste for CO_2 Capture

Xia Wang,* Wulan Zeng, Xiangjun Kong, Chunling Xin,* Yani Dong, Xiude Hu, and Qingjie Guo

Cite This: *ACS Omega* 2022, 7, 46992−47001

Read Online

ACCESS | Metrics & More | Article Recommendations | Supporting Information

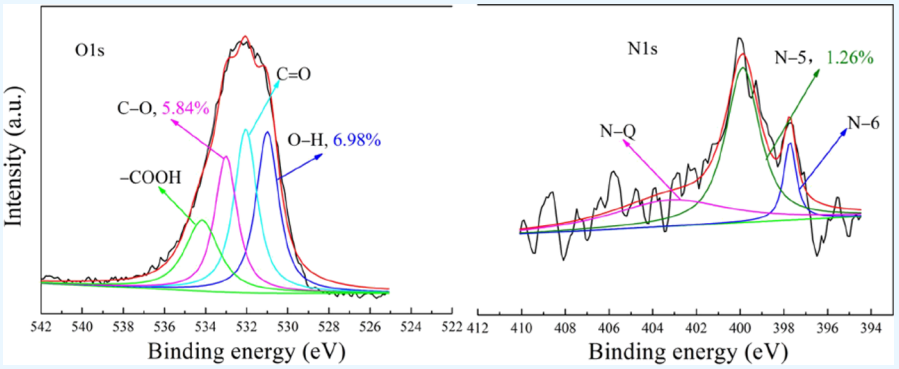

ABSTRACT: To achieve the "double carbon" (carbon peak and carbon neutrality) target, low-cost CO_2 capture at large CO_2 emission points is of great importance, during which the development of low-cost CO_2 sorbents will play a key role. Here, we chose peanut shells (P) from crop waste as the raw material and KOH and K_2CO_3 as activators to prepare porous carbons by a simple one-step activation method. Interestingly, the porous carbon showed a good adsorption capacity of 2.41 mmol/g for 15% CO_2 when the mass ratio of K_2CO_3 to P and the activation time were only 0.5 and 0.5 h, respectively, and the adsorption capacity remained at 98.76% after 10 adsorption−desorption cycle regenerations. The characterization results suggested that the activated peanut shell-based porous carbons were mainly microporous and partly mesoporous, and hydroxyl (O−H), ether (C−O), and pyrrolic nitrogen (N-5) functional groups that promoted CO_2 adsorption were formed during activation. In conclusion, KOH- and K_2CO_3-activated P, especially K_2CO_3-activated P, showed good CO_2 adsorption and regeneration performance. In addition, not only the use of a small amount of the activator but also the raw material of crop waste reduces the sorbent preparation costs and CO_2 capture costs.

1. INTRODUCTION

Achieving carbon peak and carbon neutrality targets on schedule globally is inseparable from the joint efforts of every country. As a responsible country, China has promised to strive to adopt favorable policies and measures to peak CO_2 emissions before 2030 and achieve carbon neutrality by 2060, and this undoubtedly requires arduous efforts. While realizing the tough goal, the CO_2 capture process plays a key role in large CO_2 emission points, such as coal-fired power plants, in which the CO_2 emission concentration reaches 10−15 vol %. Due to the low contact area between the gas−liquid phase and corrosive of ammonia solution absorbents to the equipments, solid sorbents are acknowledged as having more application potential.[1−9] Generally, a CO_2 adsorption capacity of 2 mmol/g for solid sorbents is thought to be suitable for application, and many studies have contributed to the large amount of research.[10−29] Usually, solid amine sorbents introduce large amounts of amino active sites onto the porous supporting materials, and their adsorption capacity of CO_2 is large;[2−6] due to their high specific surface area and tunable surface chemical property, metal organic frameworks, covalent organic frameworks, and their derivatives are widely utilized in the field of gas adsorption.[12,18,20,28,29]

Porous carbons prepared from various biomass, with the low cost of raw materials, simple preparation process, and high surface area, have also caused strong concern.[30−39] Ding and Liu used the seaweed of Sargassum and Enteromorpha as the carbon resource and prepared porous biochars by directly mixing it with the activator KOH. The maximum CO_2 adsorption capacities were 1.05 and 0.52 mmol/g, respectively, at 25 °C.[34] Rehman and Park designed microporous carbons from relatively inexpensive chitosan by a two-step method (first carbonization and then activation and synchronous N doping), which showed a developed microporous structure

Received: September 21, 2022
Accepted: November 23, 2022
Published: December 5, 2022

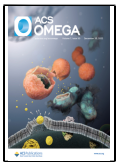

(S_{BET}: 368−2150 m^2/g; V_{micro}: 0.2255−1.3020 cm^3/g) and good CO_2 adsorption performance at 273 K and 1 bar.[30] Xu et al. prepared N-doped biochar using a waste walnut shell as the raw material by preimmersing with H_3PO_4, mixing with the nitrogen source of urea for N doping, and then activating by mixing with different activators ($ZnCl_2$, K_2CO_3, and KOH). The results showed that the sorbent activated by different activators exhibited different advantages in adsorption capacity, selectivity, and cycle performance.[35] The above study indicated that biomass and the activation method were suitable for use as the carbon resource and the synthesis process of porous carbons, respectively.

Taking the low cost into consideration, the raw material and synthesis process should be as inexpensive and simple as possible. In this study, the common waste crop peanut shell (P) in rural Shandong Province, China, was used as the carbon resource, relatively inexpensive KOH and K_2CO_3 were used as activators, and a simple one-step activation method was adopted to prepare waste crop-based porous carbons. The pore structure, functional groups, surface morphology, and carbonaceous nature of the porous carbons before and after activation were characterized, the adsorption and regeneration performances were tested, and the optimum process for synthesizing suitable porous carbon was explored.

2. EXPERIMENTAL SECTION

2.1. Materials. Peanut shells were collected from rural Weifang (Shandong, China). KOH and K_2CO_3 (AR) were purchased from Shanghai Aladdin Biochemical Technology Co., Ltd. (Shanghai, China). HCl (CR) was purchased from Far Eastern Group: Laiyang Fine Chemical Factory (Shandong, China). N_2 (99.999%) and the simulated flue gas (85% N_2 + 15% CO_2) were supplied by Weiyang Gas Co., Ltd. (Shandong, China).

2.2. Preparation of the Porous Carbons. P was first repeatedly washed with tap water and then deionized water to remove the impurities adhering to the surface and then placed in an oven to dry. The dried P was ground to a powder with a size below 100 mesh for use. The flaky KOH and K_2CO_3 were also ground to a powder to evenly mix with P.

The synthesis process of the porous carbons adopted the one-step activation method. KOH or K_2CO_3 was physically mixed with P at a certain mass ratio (0−1.5) and loaded in a tube furnace, and N_2 with a flow rate of 200 mL/min was passed through. Then, the furnace was heated to the activation temperature (650−850 °C) at a rate of 10 °C/min and kept for a certain time (0.5−1.5 h), after which the temperature was cooled below 100 °C and N_2 was turned off. The obtained powder was washed with diluted HCl and deionized water to neutral and dried at 100 °C for 16 h, which was denoted as PAC-aK_2CO_3 (KOH)-*T*-*t*, where PAC is the peanut shell-based porous carbon, a is the mass ratio of the activator to P, and *T* and *t* are the activation temperature and time, respectively.

2.3. CO_2 Adsorption and Regeneration. The CO_2 adsorption and regeneration were performed in a fixed bed reactor with the inner diameter of the quartz tube being 0.8 cm and the length being 50 cm, with a gas chromatograph connected to the outlet of the quartz tube to synchronously record the CO_2 concentration. The solid sorbent with a mass of 1.0 g was loaded in the reactor, and N_2 was passed through for 30 min to replace the attached air. The temperature of the reactor was regulated to the adsorption temperature and kept for 30 min. Then, N_2 was switched to the simulated flue gas with a flow rate of 30 mL/min, and the CO_2 adsorption process began. The CO_2 concentration in the inlet and outlet of the reactor was denoted as C_0 and C, respectively; as the adsorption progressed, C became increasingly larger. When it was equal to C_0, the adsorption process was finished, and the equilibrium adsorption capacity was calculated from the breakthrough adsorption curves.[5]

Once the adsorption process finished, the inlet gas was switched to N_2, and the temperature was raised to 100 °C to release the adsorbed CO_2 on the sample. As the desorption progressed, C decreased, and when it was equal to 0, the desorption process was finished, and the sorbent was regenerated. In this study, the preferred sorbent was regenerated ten times.

2.4. Characterization. The N_2 adsorption−desorption isotherms of the prepared porous carbons were obtained using an ASAP 2460 (Micromeritics, USA) by N_2 physical adsorption at a critical temperature of −196 °C. The Brunauer−Emmett−Teller (BET) surface area (S_{BET}) was calculated according to the BET equation, the total pore volume (V_t) was obtained from the N_2 adsorption amount at a relative pressure of 0.994, the micropore volume (V_{micro}) was analyzed from the t-plot curve, and the pore size distribution information was collected by the density functional theory method.

The elemental composition (O and N) on the prepared porous carbons was characterized with X-ray photoelectron spectroscopy (XPS) using an EscaLab 250Xi (Thermo Scientific, USA). The surface functional groups of PAC before and after K_2CO_3 activation were characterized by Fourier transform infrared (FT-IR) spectroscopy with frequencies ranging from 500 to 4000 cm^{-1}. Powder X-ray diffraction (XRD) patterns were obtained using an ASAP 2020 V4.01 X-ray diffractometer with Cu Ka radiation (k = 0.154 nm) in the range of 2θ = 5−90°. The surface morphology of the porous carbons was examined by scanning electron microscopy (SEM) using a JSM-7500F scanning electron microscope (JEOL, Japan) at 5.0 kV.

3. RESULTS AND DISCUSSION

3.1. Characterization.

(1) The N_2 adsorption−desorption isotherms, pore size distribution curves, and textural properties of PAC before and after activation are shown in Figure 1 and Table 1. In Figure 1a, the N_2 adsorption−desorption isotherms of PAC, especially the activated PAC, suggested a sharp increase at the initial adsorption stage and then an obviously gentle increase with a narrow hysteresis loop appearing when the relative pressure was over 0.40, indicating that the pores in PAC were mainly micropores with partly mesopores,[2,36,38] which could also be clearly seen from Figure 1b and Table 1. As shown in Table 1, compared with unactivated PAC, the S_{BET}, V_t, and V_{micro} for K_2CO_3 (KOH)-activated PAC increased from 83 to 669 (626) m^2/g, 0.07 to 0.43 (0.36) cm^3/g, and 0.03 to 0.35 (0.30) cm^3/g, respectively, with the mass ratio of K_2CO_3 (KOH) to P reaching 1.5 (0.5). Comparing the pore properties of the same mass ratio of K_2CO_3 with KOH, both showed a similar effect in improving the pore channel of the peanut shell.

https://doi.org/10.1021/acsomega.2c06109
ACS Omega 2022, 7, 46992−47001

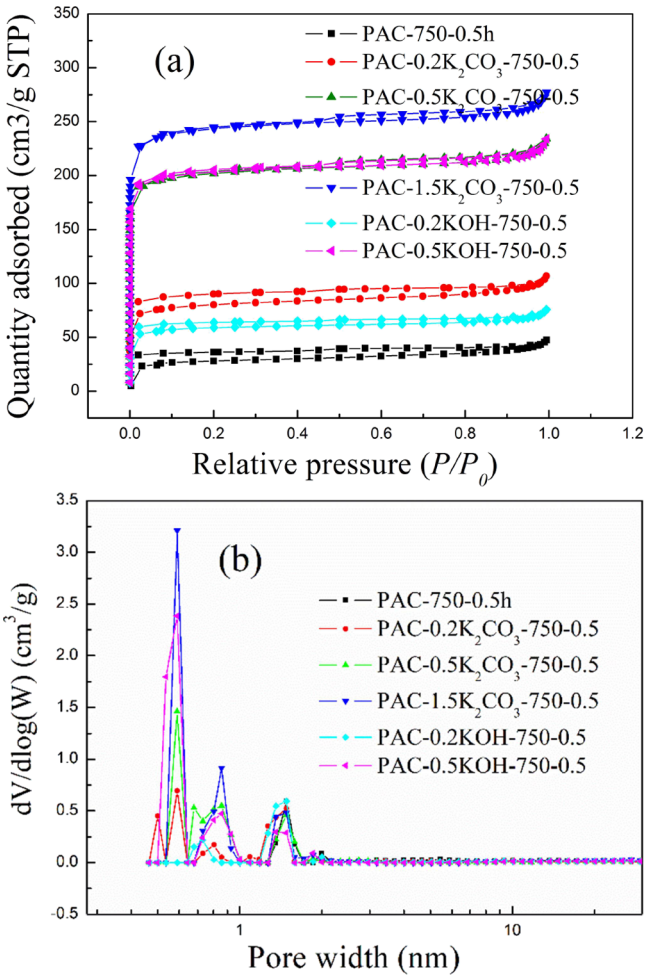

Figure 1. (a) N_2 adsorption−desorption isotherms and (b) pore size distribution curves for peanut shell-based porous carbons (PACs) before and after activation.

PAC-aK_2CO_3 (KOH)-*T*-*t*: PAC is the peanut shell-based porous carbon, a is the mass ratio of the activator to P, and *T* and *t* are the activation temperature and time, respectively.

(2) The O 1S and N 1S XPS spectra of PAC before and after activation are separately shown in Figure 2a−f and a′−f′, respectively, and the peak area ratios of different O and N species are displayed in Tables 2 and 3, respectively.

Before and after K_2CO_3 or KOH activation, the O 1S spectra were all divided into four peaks at 530.47, 531.46, 532.38, and 533.32 eV, which belonged to O−H (hydroxyl groups), C═O (ketone, carbonyl, or lactone groups), C−O (alcohol or ether groups), and −COOH (carboxyl groups), respectively;[33,34] after K_2CO_3 and KOH activation, the peak area ratio for O-containing groups obviously increased, especially the ratios of O−H and C−O groups that favor CO_2 adsorption,[34] which were 7.27 and 5.12 atom % in PAC-0.2K_2CO_3-750-0.5, 6.98 and 5.84 atom % in PAC-0.5K_2CO_3-750-0.5, 7.59 and 5.37 atom % in PAC-0.2KOH-750-0.5, and 5.38 and 5.48 atom % in PAC-0.5KOH-750-0.5, respectively, all much higher than that of PAC-750-0.5.

Before and after K_2CO_3 or KOH activation, the N 1S spectra were all divided into three peaks at 397.64, 399.98, and 402.98 eV, which were attributed to N-6 (pyridinic nitrogen), N-5 (pyrrolic nitrogen), and N-Q (quaternary nitrogen), respectively.[14,33,35] Despite the reduction of N-containing groups with activation processing, N-5, which favors CO_2 adsorption,[35] still occupied an absolute proportion in K_2CO_3-activated P, and the ratio was 1.26 atom % in PAC-0.5 K_2CO_3-750-0.5. However, for the KOH-activated peanut shell, N-5, which favors CO_2 adsorption, did not occupy an obvious proportion, and the ratio was only 0.59 atom % in PAC-0.5KOH-750-0.5.

In short, K_2CO_3 activation developed more O- and N-containing groups than KOH activation, which favored CO_2 adsorption.

(3) Figure 3 presents the FT-IR spectra of PAC before and after K_2CO_3 activation. The peak at 3437 cm^{-1} is attributed to the stretching vibration of O−H and N−H,[33] the peak at 1619 cm^{-1} belongs to the N−H in plane deformation,[40] and the peaks at 1450 and 1063 cm^{-1} are due to the C═O stretching vibration of carbonyl and the C−O stretching mode of carboxylic acid, respectively.[34] The appearance of the upper peaks is consistent with the XPS characterization results.

(4) The XRD patterns are shown in Figure 4 to elaborate the carbonaceous property of the PACs before and after K_2CO_3 activation. The broad peaks at ∼23 and ∼43° are usually identified as reflections from the (002) and (100) planes of the hexagonal graphite structure, respectively.[15,32,41,42] The broad peak at 23° suggests the amorphous property of the prepared samples, and the weaker peak intensity for PAC-1.5K_2CO_3-750-0.5 suggests obviously poor crystallinity, which was due to the destruction of graphite layers by K_2CO_3 etching. In addition, no crystallinity of K_2CO_3 appeared, suggesting that K_2CO_3 was completely removed.

(5) Figure 5 shows the SEM micrographs to explain the surface morphology of the peanut hell-based porous carbons before and after K_2CO_3 activation. From Figure 5a, the unactivated PAC displayed sheet-like structure cracks, but for the K_2CO_3-activated peanut shell, developed porous structures were formed. For PAC-0.2K_2CO_3-750-0.5, the surface exhibited layered wedge holes, but with the increase in the K_2CO_3 ratio, the holes became interconnected, especially for PAC-1.5K_2CO_3-

Table 1. Textural Pore Properties for PAC before and after Activation

sample	S_{BET} (m^2/g)	V_t (cm^3/g)	V_{micro} (cm^3/g)	microporosity (%)	average pore diameter (nm)
PAC-750-0.5h	83	0.07	0.03	42.86	3.56
PAC-0.2K_2CO_3-750-0.5	229	0.16	0.11	68.75	2.88
PAC-0.5K_2CO_3-750-0.5	566	0.36	0.29	80.56	2.56
PAC-1.5K_2CO_3-750-0.5	669	0.43	0.35	81.40	2.57
PAC-0.2KOH-750-0.5	182	0.12	0.08	66.67	2.87
PAC-0.5KOH-750-0.5	626	0.36	0.30	83.33	2.54

https://doi.org/10.1021/acsomega.2c06109
ACS Omega 2022, 7, 46992−47001

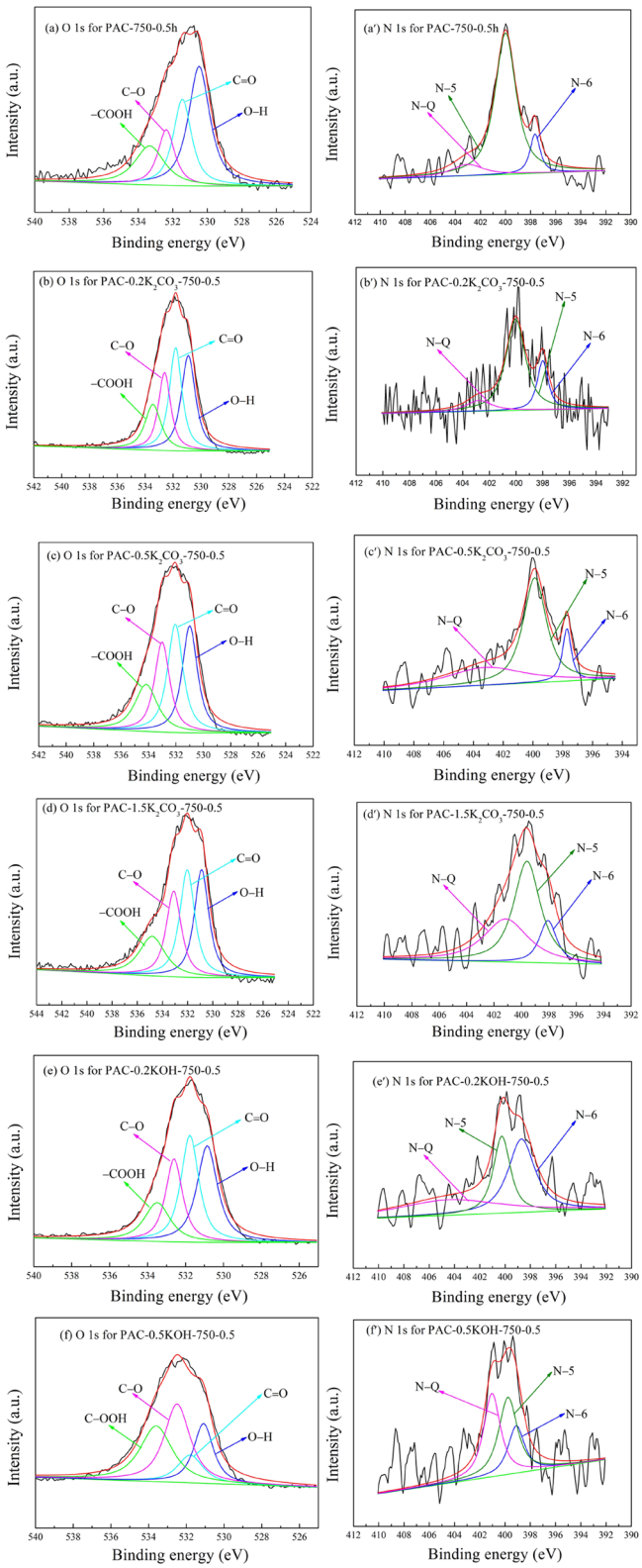

Figure 2. (a–f) O 1S and (a′–f′) N 1S XPS spectra for PAC before and after activation.

750-0.5, in which highly dense pores were observed. With the increase in the K_2CO_3 ratio, more K_2CO_3 participated in etching, metallic K intercalation, and carbon gasification, so more developed pores were formed.[32,43] The SEM characterization results were consistent with the BET characterization.

3.2. Effect of Activation Temperature on CO_2 Adsorption on PAC. The activation temperature affects the extent of K_2CO_3 and KOH etching, surface functional group development, and pore formation. The mass ratio of the activator to P and the activation time were fixed at 1:1 and 1 h, respectively, to investigate the effect of activation temperature on CO_2 adsorption on PAC at 20 °C.

The breakthrough adsorption curves for KOH- and K_2CO_3-activated peanut shells are separately shown in Figures S1a and S2a, and the equilibrium adsorption capacities for both are shown in Figure 6. With the increase in temperature from 650 to 850 °C, the breakthrough adsorption curve moved right and then left, and the greater the curve moved to the right, the higher the adsorption performance was, so the adsorption capacity suggested a trend of increasing first and then decreasing, as shown in Figure 6. When the temperature was 750 °C, the equilibrium adsorption capacities for PAC-KOH-750-1 and PAC-K_2CO_3-750-1 were 2.00 and 2.41 mmol/g, respectively. Compared with KOH-activated P prepared under the same conditions, K_2CO_3-activated P showed a higher adsorption capacity, which might be related to the greater number of O–H, C–O, and N-5 groups.

Next, the activation temperature was fixed at 750 °C, and the activation time was fixed at 1 h to further investigate the effect of the mass ratio of the activator to P on CO_2 adsorption on PAC at 20 °C.

3.3. Effect of the Mass Ratio of the Activator to P on CO_2 Adsorption on PAC. The breakthrough adsorption curves for PAC with different mass ratios of KOH and K_2CO_3 to P during activation are shown in Figures S1b and S2b, and the corresponding equilibrium adsorption capacity is shown in Figure 7. For both KOH and K_2CO_3 activation, the breakthrough adsorption curves moved right first and then left, and the adsorption capacity first increased and then decreased. When the mass ratio of KOH and K_2CO_3 to P was 0.5–1, PAC exhibited a maximum adsorption capacity, which was 1.99–2.00 and 2.41 mmol/g, respectively. From the BET characterization results of K_2CO_3-activated P, the greater the mass ratio of K_2CO_3 was, the larger the S_{BET}, V_t, and V_{micro} were; however, from the XPS results, the largest amounts of O- and N-containing functional groups, especially O–H, C–O, and N-5, which favor CO_2 adsorption, appeared when the mass ratio was 0.5:1. In addition, more K_2CO_3 increased the preparation costs and post-treatment process (especially washing process) of the porous carbons. Therefore, the K_2CO_3 mass ratio was not continuously increased to further study.

Next, the activation temperature and the mass ratio of the activator to P were set as 750 °C and 0.5:1, respectively, to further investigate the effect of activation time on CO_2 adsorption on PAC at 20 °C.

3.4. Effect of Activation Time on CO_2 Adsorption on PAC. The breakthrough adsorption curves of PAC after KOH and K_2CO_3 activation for different activation times are shown in Figures S1c and S2c, respectively, and the corresponding equilibrium adsorption capacity is displayed in Figure 8. For both KOH- and K_2CO_3-activated P, the adsorption time did not have much effect on the breakthrough adsorption curves or the equilibrium adsorption capacity, which is a sign that the

https://doi.org/10.1021/acsomega.2c06109
ACS Omega 2022, 7, 46992–47001

Table 2. Peak Area Ratios of Different O Species in PAC before and after Activation

sample	O atom %	O species ratio, %				−OH atom %	−C═O atom %	C−O atom %	−COOH atom %
		−OH	−C═O	C−O	−COOH				
PAC-750-0.5h	9.60	41.06	25.24	15.12	18.58	3.94	2.42	1.45	1.78
PAC-0.2K_2CO_3-750-0.5	23.33	31.15	29.90	21.94	17.00	7.27	6.98	5.12	3.97
PAC-0.5K_2CO_3-750-0.5	24.62	28.35	29.31	23.71	18.63	6.98	7.22	5.84	4.59
PAC-1.5K_2CO_3-750-0.5	14.61	28.61	29.28	23.43	18.68	4.18	4.28	3.42	2.73
PAC-0.2KOH-750-0.5	24.06	31.54	30.24	22.32	15.90	7.59	7.28	5.37	3.83
PAC-0.5KOH-750-0.5	21.33	25.22	30.90	25.70	18.18	5.38	6.59	5.48	3.88

Table 3. Peak Area Ratios of Different N Species in PAC before and after Activation

sample	N atom %	N species ratio, %			N-6 atom %	N-5 atom %	N-Q atom %
		N-6	N-5	N-Q			
PAC-750-0.5h	2.68	10.69	79.79	9.52	0.29	2.14	0.26
PAC-0.2K_2CO_3-750-0.5	1.20	20.70	68.68	10.62	0.25	0.82	0.13
PAC-0.5K_2CO_3-750-0.5	2.22	10.68	56.83	32.49	0.24	1.26	0.72
PAC-1.5K_2CO_3-750-0.5	2.07	13.55	50.42	36.03	0.28	1.04	0.75
PAC-0.2KOH-750-0.5	1.95	39.76	26.63	33.61	0.78	0.52	0.66
PAC-0.5KOH-750-0.5	1.47	21.34	39.82	38.85	0.31	0.59	0.57

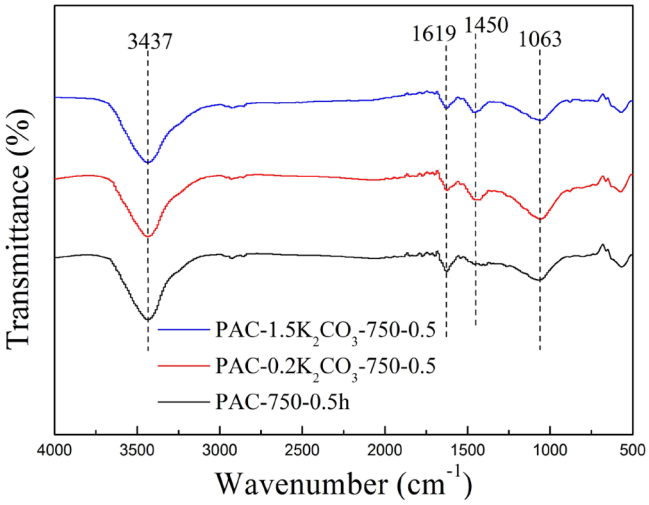

Figure 3. FT-IR spectra for PAC before and after K_2CO_3 activation.

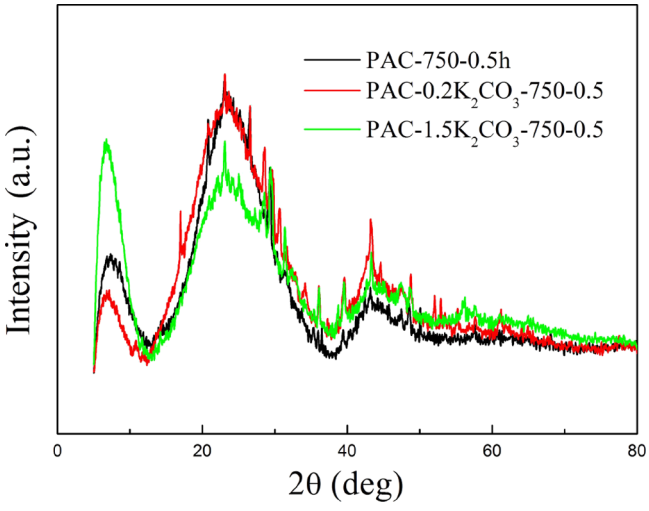

Figure 4. XRD spectra for PAC before and after K_2CO_3 activation.

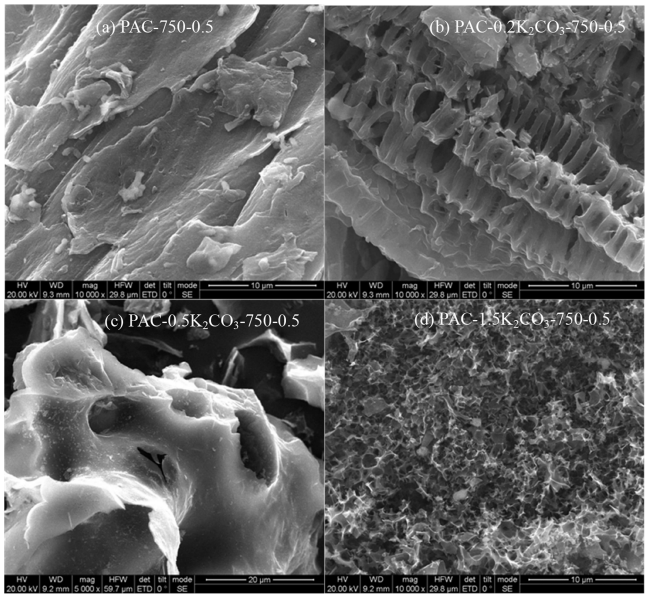

Figure 5. (a−d) SEM images of PAC before and after K_2CO_3 activation.

activation effect could be fulfilled in 0.5 h, and a longer time was not needed.

In conclusion, when the activation temperature and time were 750 °C and 0.5 h, respectively, and the mass ratio of the activator to P was 0.5:1, the maximum CO_2 adsorption capacity of K_2CO_3-activated PAC at 20 °C was 2.41 mmol/g, which is greater than that of ZIF-8 grafted biochar (1.80 mmol/g),[18] seaweed-based porous carbon (1.05 mmol/g),[34] and waste walnut shell-based porous carbons (0.60 mmol/g).[35] In some related studies,[15,30,32,34,35] the optimal adsorption capacity usually appeared when the activation time and mass ratio of the activator to the biomass were 1−3 h and 1−2, respectively. In contrast, the shorter activation times at high temperatures and lower mass ratios of the activator in this study reduce both the energy consumption and activation cost to a large extent.

https://doi.org/10.1021/acsomega.2c06109
ACS Omega 2022, 7, 46992−47001

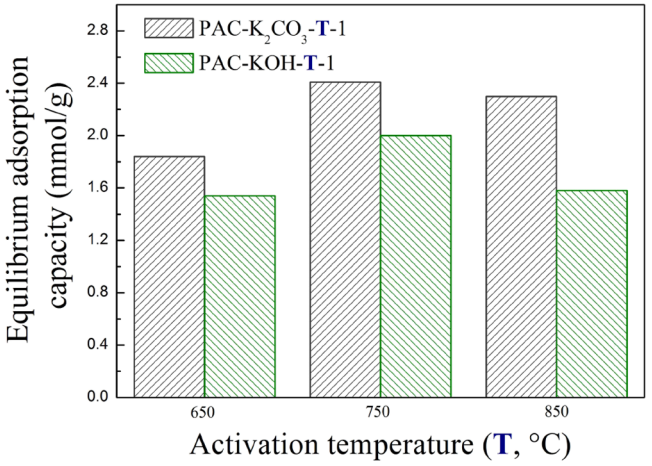

Figure 6. Equilibrium adsorption capacity of K_2CO_3- and KOH-activated PAC at different activation temperatures.

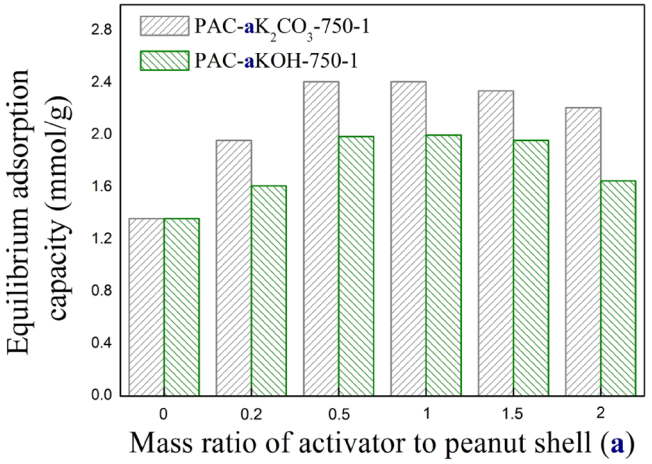

Figure 7. Equilibrium adsorption capacity of activated PAC with different mass ratios of K_2CO_3 or KOH to peanut shell (a).

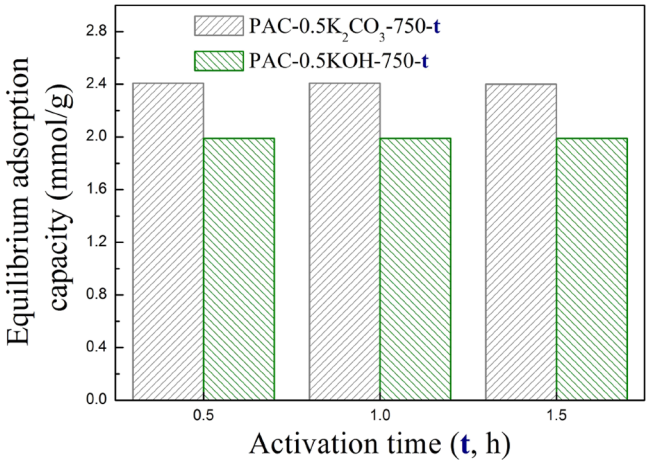

Figure 8. Equilibrium adsorption capacity of PAC after K_2CO_3 and KOH activation for different times.

In view of the slightly superior adsorption performance of K_2CO_3-activated PAC compared to KOH-activated PAC, PAC-0.5K_2CO_3-750-0.5 was further studied to investigate the adsorption mechanism and kinetics.

3.5. CO_2 Adsorption Property of PAC-0.5K_2CO_3-750-0.5. To further study the adsorption property of the activated PAC, the breakthrough adsorption curves and corresponding adsorption capacity of PAC-0.5K_2CO_3-750-0.5 at different adsorption temperatures were collected and calculated, as shown in Figures S3 and 9. With the increasing adsorption

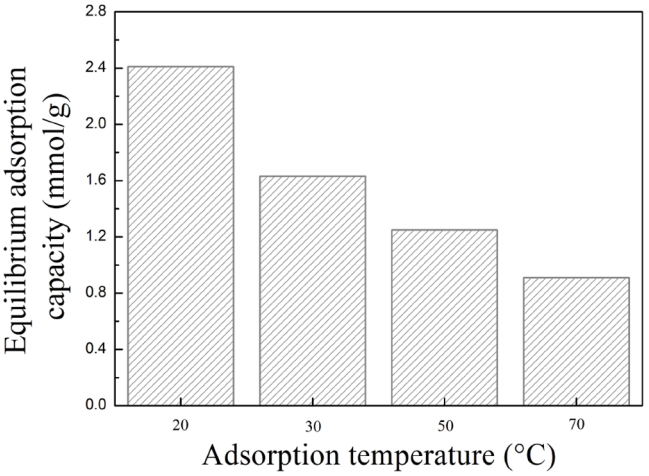

Figure 9. Equilibrium adsorption capacity of PAC-0.5K_2CO_3-750-0.5 at different adsorption temperatures.

temperature, the breakthrough adsorption curves moved left, and the corresponding adsorption capacity decreased, suggesting the physisorption characteristic of PAC-0.5K_2CO_3-750-0.5.

To explore the dependence of adsorption on the pore property and surface functional groups, the linear correlations between the adsorption capacity and S_{BET}, V_t, V_{micro}, and the total functional group (O−H, C−O, and N-5) ratio are shown in Figure 10. As shown in Figure 10a−d, the equilibrium adsorption capacity of the prepared PAC did not exhibit good linear fitting with S_{BET}, V_t, V_{micro}, and the total functional groups, with the correlation coefficient of R^2 ranging from 0.7866 to 0.8036, indicating that the CO_2 adsorption capacity did not completely depend on the pore property or the surface functional group, but the joint effects of both played important roles in the adsorption.

Generally, the higher the activation temperature and the greater the mass ratio of the activator are, the more K_2CO_3 or KOH participates in etching, metallic K intercalation, and carbon gasification from the cracks,[36] which promote the formation of pores and O- and N-containing functional groups. However, overactivation might destroy the pore structure and promote the further decomposition of functional groups, so the effects of the activation temperature and mass ratio of the activator to P were investigated above to find the optimal preparation process for PAC.

3.6. Adsorption Kinetics of the Activated PAC. The pseudo-first-order, pseudo-second-order, and Avrami models were used to fit the adsorption capacity data of PAC-0.5K_2CO_3-750-0.5 (at 20 and 30 °C) and PAC-0.5KOH-750-0.5 (at 20 °C), and the fitting curves and fitting parameters are shown in Figure 11 and Table 4, respectively. For both PAC-0.5K_2CO_3-750-0.5 and PAC-0.5KOH-750-0.5, the adsorption data all deviated from both pseudo-first-order and pseudo-second-order models but were well fitted with the Avrami model, with correlation coefficients all over 0.99. The good fitting of the Avrami model suggested that the CO_2

https://doi.org/10.1021/acsomega.2c06109
ACS Omega 2022, 7, 46992−47001

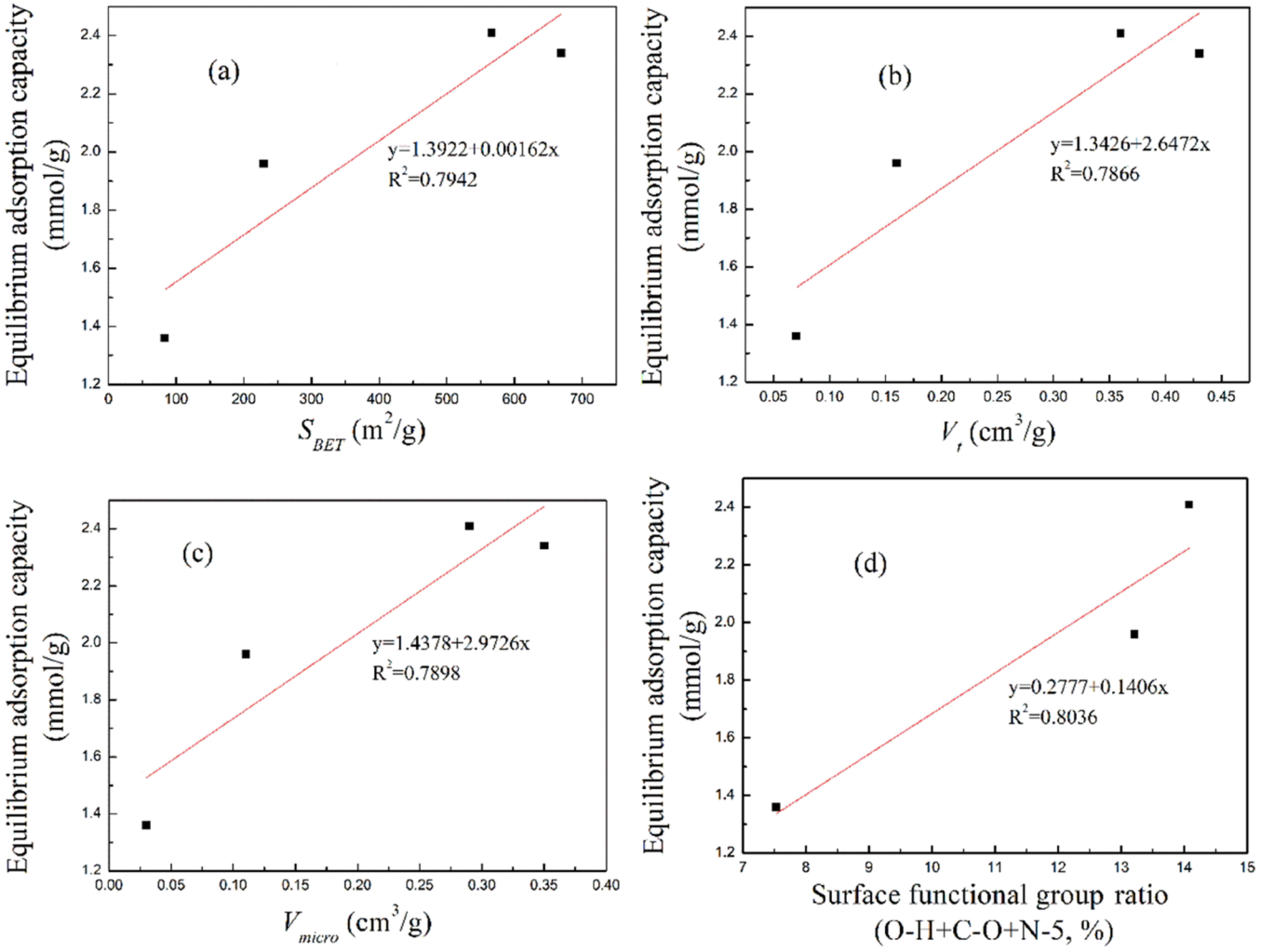

Figure 10. Linear correlation fitting between the equilibrium adsorption capacity and (a) S_{BET}, (b) V_t, (c) V_{micro}, and (d) surface functional group ratio (O−H + C−O + N-5, %).

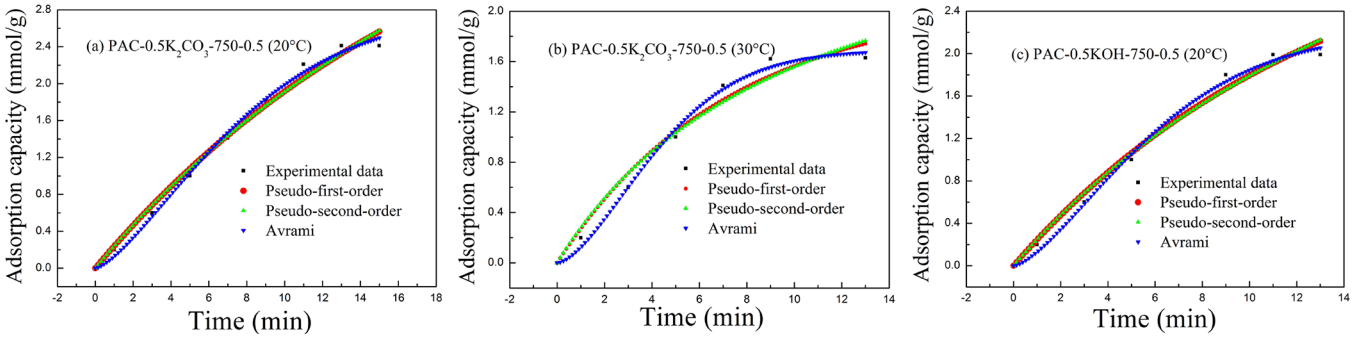

Figure 11. Kinetic fitting of PAC-0.5K_2CO_3-750-0.5 at (a) 20 °C and (b) 30 °C and (c) PAC-0.5KOH-750-0.5 at 20 °C.

adsorption on KOH- and K_2CO_3-activated P experienced not a single physisorption or chemisorption but a multiple adsorption path.[38,44]

3.7. Regeneration. Ten adsorption−desorption cycle regeneration experiments were performed to study the regeneration performance of PAC-0.5K_2CO_3-750-0.5 and PAC-0.5KOH-750-0.5, and the adsorption capacity after every regeneration is shown in Figure 12. During 10 adsorption−desorption cycles, the adsorption capacity did not show an obvious reduction and remained at 2.38 and 1.96 mmol/g after 10 regenerations, which are 98.76 and 98.49% of the fresh sample, respectively, suggesting the good regeneration performance of K_2CO_3- and KOH-activated peanut shells.

4. CONCLUSIONS

Peanut shells (P), a common crop waste in Shandong Province, China, are usually incinerated, which pollutes the environment and releases a large amount of CO_2. In this study, peanut shells were used as the raw material, KOH and K_2CO_3

https://doi.org/10.1021/acsomega.2c06109
ACS Omega 2022, 7, 46992−47001

Table 4. Kinetic Fitting Parameters for PAC-0.5K_2CO_3-750-0.5 and PAC-0.5KOH-750-0.5

kinetic model	parameter	20 °C (PAC-0.5K_2CO_3-750-0.5)	30 °C (PAC-0.5K_2CO_3-750-0.5)	20 °C (PAC-0.5KOH-750-0.5)
pseudo -first-order	q_e (mmol/g)	4.80	2.08	3.40
	k_1 (1/min))	0.0509	0.1397	0.0751
	R^2	0.9885	0.9770	0.9859
pseudo -second-order	q_e (mmol/g)	8.47	3.1694	5.79
	k_2 (g/mmol min)	0.00344	0.0305	0.00773
	R^2	0.9877	0.9716	0.9846
Avrami	q_e (mmol/g)	2.81	1.69	2.21
	k_a (1/min)	0.1155	0.1996	0.1489
	n_a	1.4188	1.5938	1.47003
	R^2	0.9939	0.9926	0.9934

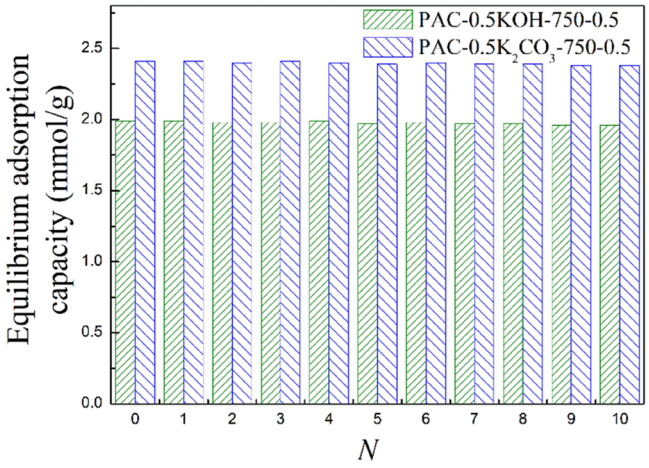

Figure 12. Equilibrium adsorption capacity of PAC-0.5KOH-750-0.5 and PAC-0.5K_2CO_3-750-0.5 after every regeneration.

were used as activators, and a one-step activation method was adopted to prepare PAC to capture CO_2 from coal-fired power plants. Compared with KOH-activated PAC, K_2CO_3-activated PAC exhibited a similar specific surface area and pore volume under the same preparation conditions but more O- and N-containing functional groups, especially O−H, C−O, and N-5, which favored CO_2 adsorption. To our surprise, the activated PAC showed a maximum adsorption capacity of 2.41 mmol/g when the mass ratio of K_2CO_3 to P and activation time were only 0.5 and 0.5 h, respectively, and the small amount of activator and the short activation time are the advantages of this work. In addition, the adsorption capacity showed no obvious reduction after 10 adsorption−desorption cycle regenerations.

The use of peanut shells and a small amount of the activator reduced the sorbent preparation costs, the short activation time reduced energy consumption, and the effective utilization of crop waste curbed environmental pollution; thus, PAC has potential as a CO_2 sorbent.

■ ASSOCIATED CONTENT

Supporting Information

The Supporting Information is available free of charge at https://pubs.acs.org/doi/10.1021/acsomega.2c06109.

Breakthrough adsorption curves for KOH- and K_2CO_3-activated peanut shells (Figures S1 and S2, respectively); breakthrough adsorption curves of PAC-0.5K_2CO_3-750-0.5 at different adsorption temperatures (Figure S3); and the XPS survey scans (Figure S4) (PDF)

■ AUTHOR INFORMATION

Corresponding Authors

Xia Wang − *Department of Chemistry and Chemical Engineering, Weifang University, Weifang 261061 Shandong, China*; orcid.org/0000-0003-2651-7166; Email: xiawangwfu@163.com

Chunling Xin − *Department of Chemistry and Chemical Engineering, Weifang University, Weifang 261061 Shandong, China*; orcid.org/0000-0002-1496-1262; Email: xinchunling0925@126.com

Authors

Wulan Zeng − *Department of Chemistry and Chemical Engineering, Weifang University, Weifang 261061 Shandong, China*; orcid.org/0000-0001-5029-6493

Xiangjun Kong − *Department of Chemistry and Chemical Engineering, Weifang University, Weifang 261061 Shandong, China*

Yani Dong − *Department of Chemistry and Chemical Engineering, Weifang University, Weifang 261061 Shandong, China*

Xiude Hu − *State Key Laboratory of High-Efficiency Utilization of Coal and Green Chemical Engineering, Ningxia University, Yinchuan 750021, China*

Qingjie Guo − *State Key Laboratory of High-Efficiency Utilization of Coal and Green Chemical Engineering, Ningxia University, Yinchuan 750021, China*

Complete contact information is available at: https://pubs.acs.org/10.1021/acsomega.2c06109

Notes

The authors declare no competing financial interest.

■ ACKNOWLEDGMENTS

The financial support from the National Natural Science Foundation of China (Grant No. 22108208), the State Key Laboratory of High-Efficiency Utilization of Coal and Green Chemical Engineering (Grant No. 2021-K02), and Weifang Science and Technology Development Plan (Grant No. 2021GX004) is gratefully acknowledged.

■ REFERENCES

(1) Smyrnioti, M.; Tampaxis, C.; Steriotis, T.; Ioannides, T. Study of CO_2 adsorption on a commercial CuO/ZnO/Al_2O_3 catalyst. *Catal. Today* **2020**, *357*, 495−502.

(2) Wang, Y.; Hu, X.; Guo, T.; Tian, W.; Hao, J.; Guo, Q. The competitive adsorption mechanism of CO_2, H_2O and O_2 on a solid amine adsorbent. *Chem. Eng. J.* **2020**, *416*, No. 129007.

(3) Lourenço, M. A. O.; Fontana, M.; Jagdale, P.; Pirri, C. F.; Bocchini, S. Improved CO_2 adsorption properties through amine functionalization of multi-walled carbon nanotubes. *Chem. Eng. J.* **2021**, *414*, 128763−128775.
(4) Wang, Y.; Guo, T.; Hu, X.; Hao, J.; Guo, Q. Mechanism and kinetics of CO_2 adsorption for TEPA-impregnated hierarchical mesoporous carbon in the presence of water vapor. *Powder Technol.* **2020**, *368*, 227−236.
(5) Wang, X.; Zeng, W.; Song, M.; Wang, F.; Hu, X.; Guo, Q.; Liu, Y. Polyetheramine improves the CO_2 adsorption behavior of tetraethylenepentamine-functionalized sorbents. *Chem. Eng. J.* **2019**, *364*, 475−484.
(6) Zhen, W.-T.; Huang, K.; Dai, S. Solvothermal and template-free synthesis of N-functionalized mesoporous polymer for amine impregnation and CO_2 adsorption. *Microporous Mesoporous Mater.* **2019**, *290*, 109653−109659.
(7) Wang, S.; Xu, Y.; Miao, J.; Liu, M.; Ren, B.; Zhang, L.; Liu, Z. Facile synthesis of microporous carbon xerogels for highly selective CO_2 adsorption. *J. Cleaner Prod.* **2020**, *253*, 120023−120031.
(8) Aquino, T. F.; Estevam, S. T.; Viola, V. O.; Marques, C. R. M.; Zancan, F. L.; Vasconcelos, L. B.; Riella, H. G.; Pires, M. J. R.; Morales-Ospino, R.; Torres, A. E. B.; Bastos-Neto, M.; Cavalcante, C. L., Jr. CO_2 adsorption capacity of zeolites synthesized from coal fly ashes. *Fuel* **2020**, *276*, 118143−118152.
(9) Liu, Y.; Hou, J. Selective adsorption of CO_2/CH_4 mixture on clay-rich shale using molecular simulations. *J. CO2 Util.* **2020**, *39*, 101143−101152.
(10) Lee, C. H.; Choi, S. W.; Yoon, H. J.; Kwon, H. J.; Lee, H. C.; Jeon, S. G.; Lee, K. B. Na_2CO_3-doped CaO-based high-temperature CO_2 sorbent and its sorption kinetics. *Chem. Eng. J.* **2018**, *352*, 103−109.
(11) Muriithi, G. N.; Petrik, L. F.; Doucet, F. J. Synthesis, characterization and CO_2 adsorption potential of NaA and NaX zeolites and hydrotalcite obtained from the same coal fly ash. *J. CO2 Util.* **2020**, *36*, 220−230.
(12) Chang, C.-W.; Kao, Y.-H.; Shen, P.-H.; Kang, P.-C.; Wang, C.-Y. Nanoconfinement of metal oxide MgO and ZnO in zeolitic imidazolate framework ZIF-8 for CO_2 adsorption and regeneration. *J. Hazard. Mater.* **2020**, *400*, 122974−122986.
(13) Ma, Z.; Yang, Z.; Zhang, H.; Liu, Z. Nitrogen-doped microporous carbon materials with uniform pore diameters: Design and applications in CO_2 and H_2 adsorption. *Microporous Mesoporous Mater.* **2020**, *296*, 109992−109998.
(14) Rehman, A.; Park, S.-J. Environmental remediation by microporous carbon: An efficient contender for CO_2 and methylene blue adsorption. *J. CO2 Util.* **2019**, *34*, 656−667.
(15) Kuwahara, Y.; Hanaki, A.; Yamashita, H. A direct conversion of blast furnace slag to a mesoporous silica-calcium oxide composite and its application in CO_2 captures. *Green Chem.* **2020**, *22*, 3759−3768.
(16) Zhao, H.; Zhao, N.; Wang, Q.; Li, F.; Wang, F.; Fan, S.; Matus, E. V.; Ismagilov, Z. R.; Li, L.; Xiao, F. Adsorption equilibrium and kinetics of CO2 on mesocellular foams modified HKUST-1: Experiment and simulation. *J. CO2 Util.* **2021**, *44*, 101415−101424.
(17) Dong, H.; Cui, H.; Zhou, Z. Promoting effects of Li_3PO_4 and $CaCO_3$ on the intermediate-temperature CO_2 adsorption over molten $NaNO_3$ promoted MgO-based sorbents. *Chem. Eng. J.* **2022**, *442*, 136133−136142.
(18) Zhang, J.; Huang, D.; Shao, J.; Zhang, X.; Zhang, S.; Yang, H.; Chen, H. A new nitrogen-enriched biochar modified by ZIF-8 grafting and annealing for enhancing CO_2 adsorption. *Fuel Process. Technol.* **2022**, *231*, 107250−107259.
(19) Xiao, J.; Sitamraju, S.; Janik, M. J. CO_2 adsorption thermodynamics over N-substituted/grafted graphanes: a DFT study. *Langmuir* **2014**, *30*, 1837−1844.
(20) Tuci, G.; Iemhoff, A.; Rossin, A.; Yakhvarov, D.; Gatto, M. F.; Balderas-Xicohténcatl, R.; Zhang, L.; Hirscher, M.; Palkovits, R.; Pham-Huu, C.; Giambastiani, G. Tailoring morphological and chemical properties of covalent triazine frameworks for dual CO_2 and H_2 adsorption. *Int. J. Hydrogen Energy* **2022**, *47*, 8434−8445.
(21) Yang, S.-T.; Kim, J.-Y.; Kim, J.; Ahn, W.-S. CO_2 capture over amine-functionalized MCM-22, MCM-36 and ITQ-2. *Fuel* **2012**, *97*, 435−442.
(22) Benedetti, A.; Ilavsky, J.; Segre, C.; Strumendo, M. Analysis of textural properties of CaO-based CO_2 sorbents by ex situ USAXS. *Chem. Eng. J.* **2019**, *355*, 760−776.
(23) Jayakumar, A.; Gomez, A.; Mahinpey, N. Post-combustion CO_2 capture using solid K_2CO_3: discovering the carbonation reaction mechanism. *Appl. Energy* **2016**, *179*, 531−543.
(24) Handoko, A. D.; Khoo, K. H.; Tan, T. L.; Jin, H.; Seh, Z. W. Establishing new scaling relations on two-dimensional MXenes for CO_2 electroreduction. *J. Mater. Chem. A* **2018**, *6*, 21885−21890.
(25) Ghosh, S.; Sarathi, R.; Ramaprabhu, S. Magnesium oxide modified nitrogen-doped porous carbon composite as an efficient candidate for high pressure carbon dioxide capture and methane storage. *J. Colloid Interface Sci.* **2019**, *539*, 245−256.
(26) Raganati, F.; Chirone, R.; Ammendola, P. CO_2 capture by temperature swing adsorption: working capacity as affected by temperature and CO_2 partial pressure. *Ind. Eng. Chem. Res.* **2020**, *59*, 3593−3605.
(27) Meroni, D.; Presti, L. L.; Liberto, G. D.; Ceotto, M.; Acres, R. G.; Prince, K. C.; Bellani, R.; Soliveri, G.; Ardizzone, S. A close look at the structure of the TiO_2-APTES interface in hybrid nanomaterials and its degradation pathway: an experimental and theoretical study. *J. Phys. Chem. C* **2017**, *121*, 430−440.
(28) Zhu, Y.; Zhu, D.; Yan, Q.; Gao, G.; Xu, J.; Liu, Y.; Alahakoon, S. B.; Rahman, M. M.; Ajayan, P. M.; Egap, E.; Verduzco, R. Metal oxide catalysts for the synthesis of covalent organic frameworks and one-step preparation of covalent organic framework-based composites. *Chem. Mater.* **2021**, *33*, 6158−6165.
(29) Dey, K.; Pal, M.; Rout, K. C.; Kunjattu, H. S.; Das, A.; Mukherjee, R.; Kharul, U. K.; Banerjee, R. Selective molecular separation by interfacially crystallized covalent organic framework thin films. *J. Am. Chem. Soc.* **2017**, *139*, 13083−13091.
(30) Rehman, A.; Park, S.-J. From chitosan to urea-modified carbons: Tailoring the ultra-microporosity for enhanced CO_2 adsorption. *Carbon* **2020**, *159*, 625−637.
(31) Serafin, J.; Baca, M.; Biegun, M.; Mijowska, E.; Kaleńczuk, R. J.; Sreńscek-Nazzal, J.; Michalkiewicz, B. Direct conversion of biomass to nanoporous activated biocarbons for high CO_2 adsorption and supercapacitor applications. *Appl. Surf. Sci.* **2019**, *497*, 143722−143730.
(32) Rehman, A.; Heo, Y.-J.; Nazir, G.; Park, S.-J. Solvent-free, one-pot synthesis of nitrogen-tailored alkali-activated microporous carbons with an efficient CO_2 adsorption. *Carbon* **2021**, *172*, 71−82.
(33) Zhang, L.; Tang, S.; He, F.; Liu, Y.; Mao, W.; Guan, Y. Highly efficient and selective capture of heavy metals by poly(acrylic acid) grafted chitosan and biochar composite for wastewater treatment. *Chem. Eng. J.* **2019**, *378*, 122215−122231.
(34) Ding, S.; Liu, Y. Adsorption of CO_2 from flue gas by novel seaweed-based KOH-activated porous biochars. *Fuel* **2020**, *260*, 116382−116391.
(35) Xu, Y.; Yang, Z.; Zhang, G.; Zhao, P. Excellent CO_2 adsorption performance of nitrogen-doped waste biocarbon prepared with different activators. *J. Cleaner Prod.* **2020**, *264*, 121645−121654.
(36) Wang, X.; Zeng, W.; Liu, W.; Cao, X.; Hou, C.; Ding, Q.; Lu, Y. CO_2 adsorption of lignite chars after one-step activation. *New J. Chem.* **2020**, *44*, 13755−13763.
(37) Sarwar, A.; Ali, M.; Khoja, A. H.; Nawar, A.; Waqas, A.; Liaquat, R.; Naqvi, S. R.; Asjid, M. Synthesis and characterization of biomass-derived surface-modified activated carbon for enhanced CO_2 adsorption. *J. CO2 Util.* **2021**, *46*, 101476−101489.
(38) Wang, X.; Wang, D.; Song, M.; Xin, C.; Zeng, W. Tetraethylenepentamine-modified activated semicoke for CO_2 capture from flue gas. *Energy Fuel* **2017**, *31*, 3055−3061.
(39) Pramanik, P.; Patel, H.; Charola, S.; Neogi, S.; Maiti, S. High surface area porous carbon from cotton stalk agro-residue for CO_2 adsorption and study of techno-economic viability of commercial production. *J. CO2 Util.* **2021**, *45*, 101450−101461.

https://doi.org/10.1021/acsomega.2c06109
ACS Omega 2022, 7, 46992−47001

(40) Chen, J.; Yang, J.; Hu, G.; Hu, X.; Li, Z.; Shen, S.; Radosz, M.; Fan, M. Enhanced CO_2 capture capacity of nitrogen-doped biomass-derived porous carbons. *ACS Sustainable Chem. Eng.* **2016**, *4*, 1439−1445.
(41) Liu, J.; Zhang, T.; Wang, Z.; Dawson, G.; Chen, W. Simple pyrolysis of urea into graphitic carbon nitride with recyclable adsorption and photocatalytic activity. *J. Mater. Chem.* **2011**, *21*, 14398−14401.
(42) Wang, J.; Kaskel, S. KOH activation of carbon-based materials for energy storage. *J. Mater. Chem.* **2012**, *22*, 23710−23725.
(43) Sevilla, M.; Fuertes, A. B. Sustainable porous carbons with a superior performance for CO_2 capture. *Energy Environ. Sci.* **2011**, *4*, 1765−1771.
(44) Cestari, A. R.; Vieira, E. F. S.; Vieira, G. S.; Almeida, L. E. The removal of anionic dyes from aqueous solutions in the presence of anionic surfactant using aminopropyl silica-a kinetic study. *J. Hazard. Mater.* **2006**, *138*, 133−141.

https://doi.org/10.1021/acsomega.2c06109
ACS Omega 2022, 7, 46992−47001